photonics

MDPI

Article

Compression Optical Coherence Elastography for Assessing Elasticity of the Vaginal Wall under Prolapse after Neodymium Laser Treatment

Ekaterina Gubarkova [1,2,*], Arseniy Potapov [1], Darya Krupinova [1,3], Ksenia Shatilova [4], Maria Karabut [1], Andrey Khlopkov [4], Maria Loginova [1,2], Aleksander Sovetsky [5], Vladimir Zaitsev [5], Stefka Radenska-Lopovok [1,6], Natalia Gladkova [1], Gennady Grechkanev [1] and Marina Sirotkina [1,2]

[1] Institute of Experimental Oncology and Biomedical Technologies, Privolzhsky Research Medical University, 10/1 Minin and Pozharsky Sq., 603950 Nizhny Novgorod, Russia
[2] Center of Photonics, Lobachevsky State University of Nizhny Novgorod, 23 Gagarin Avenue, 603022 Nizhny Novgorod, Russia
[3] Nizhny Novgorod Regional Oncologic Hospital, 11/1 Delovaya St., 603126 Nizhny Novgorod, Russia
[4] "MeLSyTech" Ltd., 11D Igumnovskoe Shosse, 603901 Nizhny Novgorod, Russia
[5] Institute of Applied Physics of the RAS, 46 Ulyanova St., 603950 Nizhny Novgorod, Russia
[6] Institute of Clinical Morphology and Digital Pathology, I.M. Sechenov First Moscow State Medical University, 8-2 Trubetskaya St., 119991 Moscow, Russia
* Correspondence: kgybarkova@mail.ru

Abstract: Early stages of pelvic organ prolapses are mainly associated with the pelvic floor disfunction as a result of elasticity changes in the connective tissues including the vaginal wall. In this study, for the first time we used a compression optical coherence elastography (C-OCE) method for assessing elasticity of the vaginal wall under prolapse conditions after intravaginal neodymium (Nd:YAG) laser treatment. C-OCE was used for a comparative ex vivo study of vaginal wall average values of stiffness (elastic Young's modulus) in patients with age norm (n = 6), stage I–II prolapse (n = 5) without treatment and stage I–II prolapse post 1–2 months Nd:YAG laser treatment (n = 10). To verify the C-OCE data, the structural features of the submucosal connective tissue were identified morphometrically by Van Gieson staining using quantitative textural analysis of the state of collagen bundles. The results of a comparative evaluation of C-OCE and histological images demonstrate a statistically significant tissue stiffness decrease in vaginal wall prolapse compared to the age norm (73.5 ± 18.9 kPa vs. 233.5 ± 48.3 kPa; $p < 0.05$). This agrees with the histologically revealed increase in the space between the bundles of collagen fibers, which leads to a decrease in the uniformity of their arrangement. After Nd:YAG laser treatment, we observed statistically significant connective tissue stiffness increase compared to vaginal wall prolapse without treatment (152.1 ± 19.2 kPa vs. 73.5 ± 18.9 kPa; $p < 0.05$), which was associated with an increase in the local thickness of the collagen bundles, a change in their orientation, and an increase in the uniformity of their arrangement. The obtained results indicate that the C-OCE can be a robust method for detecting the early stages of vaginal wall prolapse and assessing the elastic modulus increase in the vaginal wall after laser treatment.

Keywords: pelvic organ prolapse (POP); vaginal wall prolapse; submucosal connective tissue; collagen; neodymium (Nd:YAG) laser treatment; compression optical coherence elastography (C-OCE)

check for updates

Citation: Gubarkova, E.; Potapov, A.; Krupinova, D.; Shatilova, K.; Karabut, M.; Khlopkov, A.; Loginova, M.; Sovetsky, A.; Zaitsev, V.; Radenska-Lopovok, S.; et al. Compression Optical Coherence Elastography for Assessing Elasticity of the Vaginal Wall under Prolapse after Neodymium Laser Treatment. *Photonics* **2023**, *10*, 6. https://doi.org/10.3390/photonics10010006

Received: 3 November 2022
Revised: 14 December 2022
Accepted: 15 December 2022
Published: 22 December 2022

1. Introduction

Pelvic organ prolapse (POP) is a common urogenital condition affecting roughly 25–50% of women worldwide over the age of 40 [1–3]. This medical condition can have a significant impact on a patient's quality of life secondary to symptoms of pelvic pressure, vaginal bulge, as well as urinary and bowel dysfunction. POP can involve descent of one or more of the anterior vaginal walls, posterior vaginal wall, vaginal apex (vaginal vault or cuff

scar after hysterectomy) or uterus (cervix), although it comprises a combination of these in many cases [4,5]. Despite the introduction of new diagnostic methods and the improvement of surgical techniques, the frequency of relapses and unsatisfactory treatment remains high. Almost 30% of pelvic floor surgeries are performed due to disease recurrence [3]. Diagnosis of the late stages of POP in women in most cases is not difficult and is based on clinical methods. However, the disadvantages of the clinical methods include the difficulty of detecting the earliest degrees of prolapse, in some cases insufficient objectivity in assessing the degree of prolapse, and the lack of possibility of comparative analysis in dynamics. For early diagnosis of the disease, it is important to determine the initial signs of destruction of the elastic and collagen fibers of the vaginal wall. Today, determination of the quantity and condition of elastic and collagen fibers in the connective tissue of the vaginal wall is possible only with a biopsy followed by morphological and immunohistochemical analysis. Currently, there are no diagnostic methods for the preclinical and asymptomatic forms, and the traditional methods of pelvic organ examination, including ultrasound and magnetic resonance imaging, indicate that the severity of objectively identified structural and functional disorders do not correspond to the clinical manifestations of the disease. At the same time, it is known that changes in the biomechanical properties of the vaginal wall, connective tissues, and muscles are thought to be significant factors in the development of POP [6,7]. Currently, the number of publications on ultrasound or magnetic resonance elastography for visualization and assessment of biomechanical properties of soft tissue is increasing [8–13]. However, resolution of those elastographic methods is insufficient for reliable diagnostics. The recently developed elastographic techniques based on optical coherence tomography (OCT) enable much higher (sub-millimeter) resolution for assessing the biomechanical properties of vaginal tissues, which can allow one to assess not only changes in elasticity in early stages of the prolapse, but also the restored elasticity after using various treatment approaches. It should be pointed out that OCT already proved to be one of the most successful imaging techniques for various clinical applications [14–16]. OCT enables micrometer-scale resolution (typically, 2–8 μm axially and 10–15 μm) and is a nondestructive, label-free, interferometric optical (often near-infrared) imaging technique that yields real-time 2D or 3D images of subsurface tissue structure to a depth of the order of 1.5 to 2 mm at a rather high speed (from tens kHz to millions of A-scans/s). A typical field of view is of the order of several millimeters, but a larger field of view enables even a larger imaging sizes, for example, 15 × 15 mm. The emerging OCT modalities, such as polarization-sensitive OCT, OCT-angiography and optical coherence elastography (OCE), as well as endoscopic and handheld scanning probes, significantly extend the prospects and possibilities of the application of OCT techniques to various types of tissues and organs [16,17].

The most common treatment options for POP, such as vaginal pessaries and surgery, often do not provide entirely satisfactory treatment results and cause urological problems [18,19]. In the last decade, the alternative to the traditional treatment options was provided by laser technologies, which are highly effective and minimally invasive and became widespread in the treatment of patients with gynecological and urogynecological pathology [20]. Depending on the goals of therapy, it is possible to use ablative [21–24] and non-ablative [25–27] laser exposure. Research on laser therapy generally shows successful results. However, these treatment approaches may be accompanied by pain, prolonged healing, and tissue necrosis. Thus, there is an increasing demand for the use of new types of non-ablative, laser-assisted procedures for the restoration of connective tissue in dystrophy of the vaginal mucosa and POP, which can be used in addition to surgical interventions [28].

In this study, we use an innovative, minimally invasive, and non-ablative procedure using a neodymium laser (Nd:YAG) with a wavelength of 1064 nm for the treatment of vaginal wall prolapse at early stages. It is assumed that the treatment is due to the photothermal effect. At the same time, there is no destruction of soft tissues or the associated risks of complications, as well as a long period of rehabilitation. Radiation is absorbed to a greater extent by deoxyhemoglobin and oxyhemoglobin of the microvasculature, and to a

lesser extent by water and collagen [29–31]. Absorption of laser radiation and heating of tissues leads to some damage of proteins due to the heat shock, which triggers the reaction of aseptic inflammation and onset of neocollagenogenesis and neoangiogenesis [32–34].

A number of studies showed the first results of the clinical efficacy of the Nd:YAG laser in gynecology [35–37]. However, the lack of an objective method for monitoring the efficiency of a Nd:YAG laser treatment prevents its wide clinical application. Thus, additional studies are needed to reliably assess the mechanisms of action of the new laser therapy and describe the clinical experience of its use. In this study, we demonstrate the use of OCT with a new physical modality, OCE, to evaluate restoration of the structural and functional properties of the connective tissue of the vaginal wall in the correction of the early stages of prolapse after a Nd:YAG laser treatment.

Previously, classical structural OCT was successfully used in gynecology for assessment of vaginal epithelial damage and monitoring of its treatment with nonoxynol-9 vaginal gel [38], visualization of polypropylene mesh within the vaginal wall following mesh-augmented prolapse repair [39], and detection of microstructural changes in ovarian tissue associated with ovarian cancer [40–42]. More recently, the first encouraging results of using OCT for tracking vaginal tissue changes after treatment with fractional pixel CO_2 laser therapy for genitourinary syndrome were obtained [43].

Over the past decade, one of new the modalities of the multimodal OCT, called OCE, became a high-contrast technique (with the resolution of ~tens of micrometers), which outperforms the conventional structural OCT in terms of specificity and sensitivity to some important pathological processes [44]. OCE enables visualization of absolute values of stiffness (elastic Young's or shear modulus) of mapping biological tissues [45–48]. OCE develops in two main directions: (i) the wave-based elastographic techniques [47] and (ii) quasi-static techniques based on the compression principle [46]. In this study, we used the compression OCE (C-OCE) method. Quantitative estimation of the tissue elasticity in C-OCE is based on the comparison of strain in the examined tissue and the precalibrated reference layer, which is usually made of weakly scattering silicone and is placed between the studied tissues and the OCT probe. This method was mainly used to study the stiffness (elastic Young's modulus) of ex vivo tissues in oncological processes. A high potential of the method was shown for assessing and detecting the boundaries of breast cancer [49–51], as well as for evaluating the efficiency of various methods of therapeutic treatment (chemotherapy and photodynamic therapy) of human and animal tumor tissues [52,53]. In the field of gynecology, the first positive results were obtained using OCE to characterize the elastic properties of normal and malignant human ovarian tissues with a sensitivity of 93.2% and a specificity of 83% [54].

The purpose of this study is to apply C-OCE for assessing the elasticity of freshly excised samples of vaginal wall tissue in various conditions. More specifically, we compare the vaginal wall elasticity using C-OCE in three conditions: age norm, stage I–II prolapse, and stage I–II prolapse after a course of Nd:YAG laser treatment. C-OCE demonstrates its potential in assessing the elasticity changes of the vaginal wall in prolapse without treatment and after laser treatment in view of the objective change in the structural and functional properties of the vaginal connective tissue. To uncover the mechanism of elasticity changes of the vaginal wall, a detailed comparison of the corresponding OCT and histological studies is carried out for the first time.

2. Materials and Methods

2.1. Patients and Samples

A total of up to 21 patients with stages I–II vaginal wall prolapse (according to pelvic organ prolapse quantification system (POP-Q) [55]), as well as any other pathology of pelvic organs requiring surgical intervention, were involved in the study. The patients' age ranged from 35 to 50 years old.

All patients were divided into three groups according to their pathology: age norm vaginal wall tissue without prolapse requiring surgical intervention in the pelvic area for

reasons other than prolapse (n = 5); anterior and/or posterior vaginal wall prolapse without preoperative treatment (n = 6); and anterior and/or posterior vaginal wall prolapse with laser preoperative treatment (n = 10). In all the patients with anterior and/or posterior vaginal wall prolapse, colporrhaphy was performed to correct POP. During the surgical intervention, an incisional biopsy of the vaginal wall in the region of the posterior fornix was performed, with the capture of the mucous and muscular layers for ex vivo examination by the C-OCE method and subsequent histological examination.

This study was approved by the institutional review board of the Privolzhsky Research Medical University (protocol #13 from 7 July 2021, protocol #2 from 4 February 2022). This trial was prospectively registered on Clinical trial. gov, NCT05000957, registered 11 August 2021, https://clinicaltrials.gov (accessed on 15 December 2022). All the patients included in the study provided written informed consent.

2.2. Intravaginal Laser Treatment

The laser treatment of the vagina was carried out using the "Magic Gyno" laser—a modification of the "Magic Max" laser ("MeLSyTech", Ltd., Nizhny Novgorod, Russia). The laser's technical characteristics were as follows: Nd:YAG laser type; wavelength 1064 nm; Q-switch mode; the energy of one pulse up to 1.5 mJ; the duration of one pulse 20–200 ns; the pause between pulses 30 μs.

The laser treatment included two steps: the first one involved treatment of all vaginal walls in circle with a conical mirror handpiece, the second one involved targeted treatment of specific vaginal walls (anterior, posterior, or lateral, depending on the clinical situation) with a corner mirror handpiece.

During the first step of the treatment, the laser beam with the diameter 4 mm scanned the treatment area in 4 circles on all the vaginal walls with the step of 2 mm (50% beam overlap). Total length of treatment area was 10 mm. When the handpiece was moved by 5 mm (50% treatment area overlap), the treatment was repeated. There were 3–5 repetitions of the treatment along the entire vaginal length in the first stage. In the biopsy area the characteristics of the treatment were the following: laser power was 8–19.8 W, time of 4 circles was 1–1.2 s, and repetitions of 4 circles in one area were 2–4.

During the second step of the treatment, the laser beam with the diameter of 4 mm scanned treatment area in 4 circles on the targeted vaginal wall with the step of 2 mm (50% beam overlap). The resulted diameter of the treated area was approximately 10 mm on the targeted vaginal wall. When the handpiece was moved by 5 mm (50% treatment area overlap), the treatment was repeated. There was one repetition of the treatment along the entire vaginal length for each wall (if treated) in the second stage. In the biopsy area the characteristics of the treatment were the following: laser power was 8–16.8 W, time of 4 circles was 1–1.2 s, repetitions of 4 circles in one area were 1–3.

The total energy exposition was 63–335 J in the biopsy area (approximately 10 × 10 mm) after two treatment steps in one procedure and after three laser procedures. Three laser procedures were performed with an interval of 4–6 weeks. Surgery with biopsy was performed 1–2 months after the last laser treatment. The procedure was performed without anesthesia.

2.3. Multimodal OCT Device

In this study, a spectral domain multimodal OCT system (Institute of Applied Physics of the Russian Academy of Sciences, Russia) with a central wavelength of 1310 nm, spectral width of 100 nm, and a receiving array enabling 20 kHz rate of A-scan acquisition was used as described in, e.g., [56,57]. The SLD-based 1310 nm OCT system provides shot noise limited imaging performance and offers better larger signal penetration depth in general compared with OCT at 900 nm light. Therefore, it is more suitable if the imaging range is required to be above 1 mm into the tissue. This device enables axial resolution of 10 μm, lateral resolution of 15 μm, and scanning depth of 2 mm in air. The OCT system has a flexibly orientable OCT probe based on the use of single-mode isotropic fiber optics with the use of the common path scheme. Scanning is performed in contact mode and

takes 26 s to acquire a 3D data set. From the 3D data set, two types of images (structural OCT and OCT-elastography (OCE) images) are acquired simultaneously in real time from one tissue area.

2.4. Compression OCE Imaging

Elastic properties of the vaginal wall tissue were studied in ex vivo samples using the phase-sensitive compression OCE (C-OCE) as described in [46,58–62]. The axial interframe strain was estimated by finding axial gradients of inter-frame phase variations. To estimate the phase gradients we used the "vector" method proposed in [61,62]. In this method, for finding strains, the axial gradients of inter-frame phase variations are found by operating with the complex-valued OCT signals as vectors in the complex plane. The phase is explicitly singled out only at the last step of signal processing. Finding the phase gradients using this method obviates the necessity of phase unwrapping even for supra-pixel displacements of scatterers. Additionally, the vector methods enable the possibility of amplitude weighting with simultaneous suppression of especially strong phase errors ~π rad. The vector representation also allows for flexibly tunable amplitude-weighted averaging over the chosen processing window. Due to this, contributions of noisy small-amplitude pixels can be efficiently suppressed. These features confer to the vector method exceptional robustness with respect to various noises, including the strain-induced "decorrelation" noise. These features make it possible to obtain strain maps of a decent quality even without periodic averaging. This possibility is very important for one-directional loading of the tissue, which is required for obtaining nonlinear stress–strain curves in a fairly broad strain range. An additional advantage of the vector method is its high computational efficiency, which requires only several seconds for elastographic post-processing of the OCT scans acquired during the tissue deformation. Furthermore, even real-time realization of elastographic imaging can be enabled using a "typical" desktop or even laptop computer without the necessity of parallel computations on multi-core graphical cards [63].

To quantify the elastic properties of the tissue samples, we used the reference layer of translucent silicone with pre-calibrated stiffness. This reference silicone layer was placed between the output window of the OCT probe and the surface of the studied tissue sample that was then slightly compressed by the OCT probe. The approach to OCT-image processing, developed in [58,62], made it possible to perform mapping of the compression-induced strains and quantitatively estimate the tangent Young's modulus (in kPa) for a preselected level of stress applied to the tissue. Details of this approach can be found in previous publications [53,58,62–64]. The tangent elastic Young's modulus of the tissue is defined as the ratio of incremental strain in silicone multiplied by silicone stiffness to the incremental tissue strain. The reference silicone layer used in this study had Young's modulus of 40 kPa, this value being found the most suitable for the study of vaginal wall stiffness (Young's modulus) that could range from 10 kPa to 300 kPa.

The corresponding conventional structural OCT images were displayed in a split-screen mode, and the OCE images were superimposed onto the corresponding structural B-scan. In the resultant 2D OCE image, the resolution (on the order of 1/2 of the processing-window size that was used to estimate gradients of interframe phase variations) was about 4 times lower than in the initial OCT images, i.e., ~40–50 μm in both directions. The so-obtained OCE-images were represented in the color-coded form, such that stiffer areas (those with smaller strain) are shown in blue, and softer areas, where deformation is greater, are shown in red.

It should be noted that quantitative estimates of the tangent Young's modulus for a preselected applied stress were made with averaging over the chosen region of interest (ROI). The data obtained in different measurements could be meaningfully compared due to utilization of the developed procedure of the applied stress standardization using the reference silicone layers as optical stress sensors [58,64]. Without such standardization, the intrinsic elastic nonlinearity of vaginal wall tissues may result in uncontrollable variability of the estimated elastic modulus in different measurements, and even different parts of

the same image [65]. For the quantitative estimates of tangent Young's modulus presented below, in all measurements, we used the stress range from 1 kPa to 3 kPa centered at 2 kPa. The local applied stress was estimated by measuring the strain of the reference silicone layer. In this study, along with the stress standardization technique [58], when estimating the tangent (current) Young's modulus for non-infinitesimal deformations of nonlinearly elastic samples, we applied the advanced variant of OCE with tracking of supra-pixel displacements of particles in the compressed mechanically heterogeneous samples to improve the quality of elastographic quantification as recently proposed in [66].

For comparative analysis of the stiffness (elastic Young's modulus) values for various studied conditions of the vaginal wall tissue, the ROI was chosen manually in the subepithelial layer to enable exact comparison with the histological data. The characteristic size of the ROIs was 300 × 900 μm, and usually we tried to choose the same size of ROI for different samples. During this process, several characteristics of C-OCE image evaluation were automatically calculated and displayed on a screen.

2.5. Histology Imaging and Analysis

In this study, histological examination was used to understand how the elastic properties measured by the C-OCE method correlate with the condition of the collagen bundles of the vaginal connective tissue at the age norm and their changes during the development of prolapse and after laser exposure.

To match the plane of the histological sections with the position of the OCT B-scan, the scan area was marked on the sample with histological ink. Histological samples were prepared according to the standard procedure and stained according to standard protocols with hematoxylin and eosin for preliminary assessment of tissue structure and Van Gieson's stain (Figure 1a,f) for quantitative and qualitative assessment of submucosal collagen fibers.

Histological samples were examined using the EVOS M7000 Imaging System (Thermo Fisher Scientific Inc., Waltham, MA USA) in transmitted light. The images were collected as objective-calibrated TIFFs and subsequently analyzed and processed in ImageJ/FIJI (National Institutes of Health, Bethesda, Maryland, USA) [67]. Quantitative textural analysis of collagen fibers was performed using Van Gieson's stain stained slide images. Three (random non-overlapping) 1200 × 1200 px (300 × 300 μm) ROIs were analyzed for each obtained sample of the vaginal wall, followed by calculation of the average value of the obtained data. The ROIs were localized in the subepithelial zone due to the area of analysis of the C-OCE data.

The algorithm for quantitative analysis of histological samples was as follows: First, the images were deconvoluted with the ImageJ plugin "Colour Deconvolution 3.0.3" using the methods described by Ruifrok and Johnston [68]. Color deconvolution was used to selectively isolate collagen fibers stained with fuchsins in bright pink (Figure 1b,g). The resulting 8-bit image representing dye transmittance was binorized using the Otsu thresholding algorithm [69]. Then, the local thickness of the collagen bundles was determined using the "LocalThickness 4.0.2" ImageJ plugin, following the methods described by Saito and Toriwaki, as well as Hildebrand and Rüegsegger [70,71]. Quantitative orientation measurement of collagen bundles was determined using the "OrientationJ 2.0.5" ImageJ plugin [71] based on the previously binarized images.

Quantitative evaluation of the histological samples involved obtaining the following parameters: local thickness, orientation, coherence, and energy. Local thickness is calculated as the largest sphere that fits inside the object and contains the point [71]. It represents the median value of the thickness of the collagen bundles, calculated directly from the pixel values in the resulting thickness map. Local thickness analysis with heat (color-coded) map visualization is shown in Figure 1c,h.

Orientation is the angle of the dominant eigenvector measured from the positive abscissa axis. The parameter reflects the angle of the dominant direction of collagen bundles relative to the epithelium. To measure the orientation of collagen bundles, all ROIs were oriented parallel to the border of the epithelium and submucosa (axial direction).

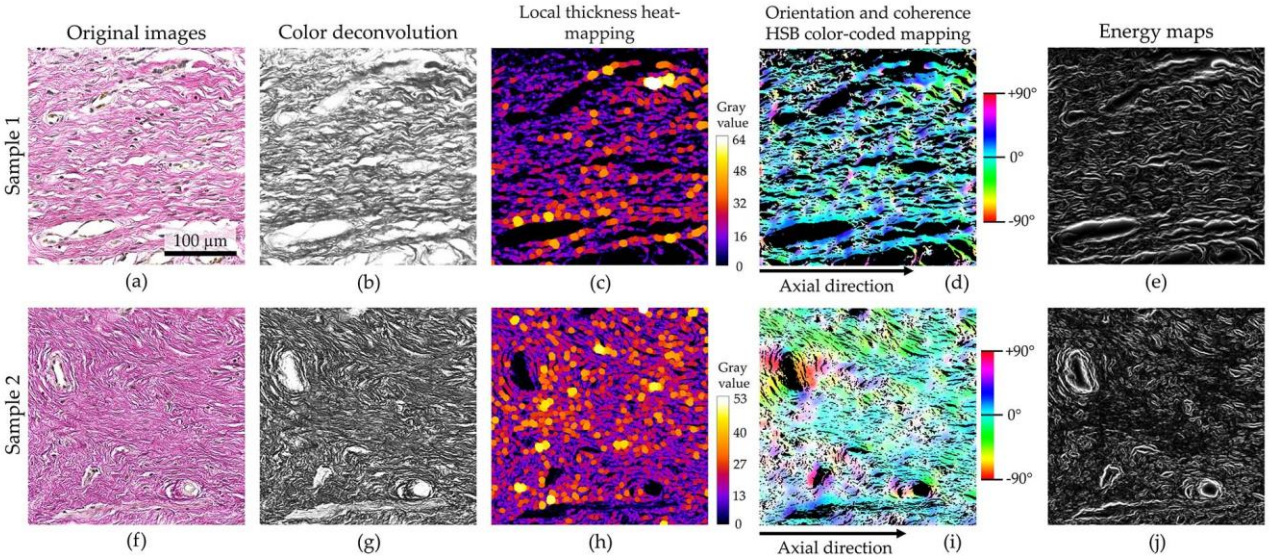

Figure 1. An example of a quantitative analysis of collagen bundles on histological sections in vaginal wall prolapse. Both samples have a different structure of collagen bundles: sample 1 (**a**–**e**) contains loose tissue with sinuous collagen bundles that have a dominant direction and are not subjected to laser preoperative treatment; sample 2 (**f**–**j**) is represented by dense tissue with numerous collagen bundles after laser preoperative treatment. (**a**,**f**)—original histological slide images; (**b**,**g**)—color deconvolution, resulting 8-bit image representing dye transmission of collagen fibers; (**c**,**h**)—local thickness analysis with heat-mapped visualization (more purple/black = less thick; more yellow/white = more thick), sample 1 has thin collagen bundles, sample 2 has thicker collagen bundles due to the increase in tissue density (10.6 ± 12.4 vs. 14.9 ± 10.2 a.u.); (**d**,**i**)—HSB color-coded map shows the orientation of collagen bundles relative to the axial direction and their coherence, hue—local orientation, saturation—coherence, brightness—original image; (**d**)—the collagen bundles in sample 1 have an orientation close to the axial direction (2.2 ± 1.9°) and high coherence (0.33 ± 0.04 a.u.) due to the alignment of the bundles; (**i**)—the collagen bundles in sample 2 deviate from the axial direction (17.8 ± 20.7°) and have reduced coherence (0.14 ± 0.03 a.u.) due to the loss of a single dominant direction; and (**e**,**j**)—the energy map shows high values at the border of collagen bundles, sample 1 has less energy than sample 2 (6234 ± 965 vs. 8639 ± 838 a.u.).

Coherence is directly proportional to the degree of ordering of the packaging of collagen bundles. The parameter reflects the degree of alignment and tortuosity, as well as the dominant direction of the bundles. Orientation and coherence hue–saturation–brightness (HSB) color-coded mapping is shown in Figure 1d,i.

Energy is a measure of the orderliness of the image, also known as uniformity (Figure 1e,j). High energy values occur when the gray level distribution has a constant or periodic form. In our case, it corresponds to a high uniformity in the collagen distribution in the field of view. Thus, this parameter indirectly reflects the density of collagen bundles in the studied ROI.

Importantly, the resolution of histological examination in the transmitted light is insufficient to reliably identify individual collagen fibers. Therefore, all calculated parameters characterize collagen bundles, which are a spatial composite of collagen fibers [72].

2.6. Statistics

The variable for statistical intergroup comparison was the average stiffness (elastic Young's modulus) calculated from the C-OCE images, as well as the indices of the subsequent tissue morphometric study (local thickness, orientation, coherence, and energy).

For quantitative comparative analysis of normal vaginal wall tissue with vaginal wall prolapse with and without laser preoperative treatment, all results are expressed as mean (±SD). Box plots were used for graphical presentation of data. The Mann–Whitney U-test

with Bonferroni correction were used to detect significant differences in numerical data between studied groups. The results were considered statistically significant if the p value was <0.05.

The Spearman's correlation coefficient (r) was calculated to determine the correlation between vaginal wall stiffness values according to the C-OCE data and local thickness, coherence, and energy parameters of collagen bundles according to histology data.

The calculations were carried out using the Statistical Package for Social Sciences 16.0 (SPSS, Chicago, IL, USA).

3. Results

3.1. Comparative Visual Assessment of the OCT and C-OCE Images for Vaginal Wall at Different Conditions: Age Norm, Stages I–II Prolapse and Prolapse after Laser Treatment

A total of 63 data sets (3 images for each patient) of structural OCT, C-OCE, and the corresponding Van Gieson's stained histology images from the 21 patients with different vaginal wall conditions were acquired and analyzed: age norm, stages I–II prolapse, and prolapse post Nd:YAG laser treatment. The main focus of our study was the submucosal connective tissue of the vaginal wall, where two zones were distinguished for visual analysis: the subepithelial zone (up to about 100 μm from the basement membrane in depth, highlighted in a black square in the Figures below) and a deeper located zone (100–500 μm from the basement membrane, highlighted in a blue square in the Figures below).

Figure 2 presents a common example of examination results for age norm conditions of the vaginal wall. Specifically, all the images display two-layer architecture with a clear boundary between epithelium and submucosal connective tissue.

In the structural OCT image (Figure 2a) uniform connective tissue with a high level of OCT-signal is visible when compared to the epithelium and signal background. This indicates the presence of a fibrous structure of collagen bundles in the connective tissue. C-OCE images of age norm vaginal wall (Figure 2b) also demonstrate a clear layered structure with relatively low stiffness values (64 $\pm$ 14 kPa) in the area of the epithelium and higher stiffness values (239 $\pm$ 51 kPa) in the area of the submucosal connective tissue. In the same image, pronounced epithelial ridges protrude into the submucosal connective tissue of the vaginal wall in the form of an uneven edge at the border with epithelium. In addition, in the C-OCE image (Figure 2b) in the area of the submucosal connective tissue, a non-uniform distribution of stiffness values is observed. We visualize two layers, such as on the histological image. Thus, the subepithelial zone with lower stiffness values (less than 200 kPa) compared to the deeper layers of the submucosa histologically corresponds to the zone with thin, intertwined collagen bundles without a specific direction (Figure 2c,(c1), arrows). The deeper layers of the submucosa with higher stiffness values (more than 200 kPa) histologically correspond to thicker and more sinuous collagen fibers, which form bundles with a predominant orientation parallel to the epithelium and practically no spaces between them (Figure 2(c2)).

Figure 3 presents a common example of examination results for the stage I–II prolapse conditions of the vaginal wall. It can be observed from the OCT (Figure 3a), C-OCE (Figure 3b), and histology (Figure 3c) images that vaginal wall prolapse is characterized by substantial differences of the structure and tissue elasticity in comparison with the age norm.

In this case, in the structural OCT image (Figure 3a), a two-layer structure with a thinned epithelium with a low OCT signal level and the submucosal connective tissue with a higher OCT signal level is visualized. However, the structural OCT image does not reflect the true state of the vaginal wall submucosal connective tissue during POP and does not allow for the distinguishing of it from the age norm.

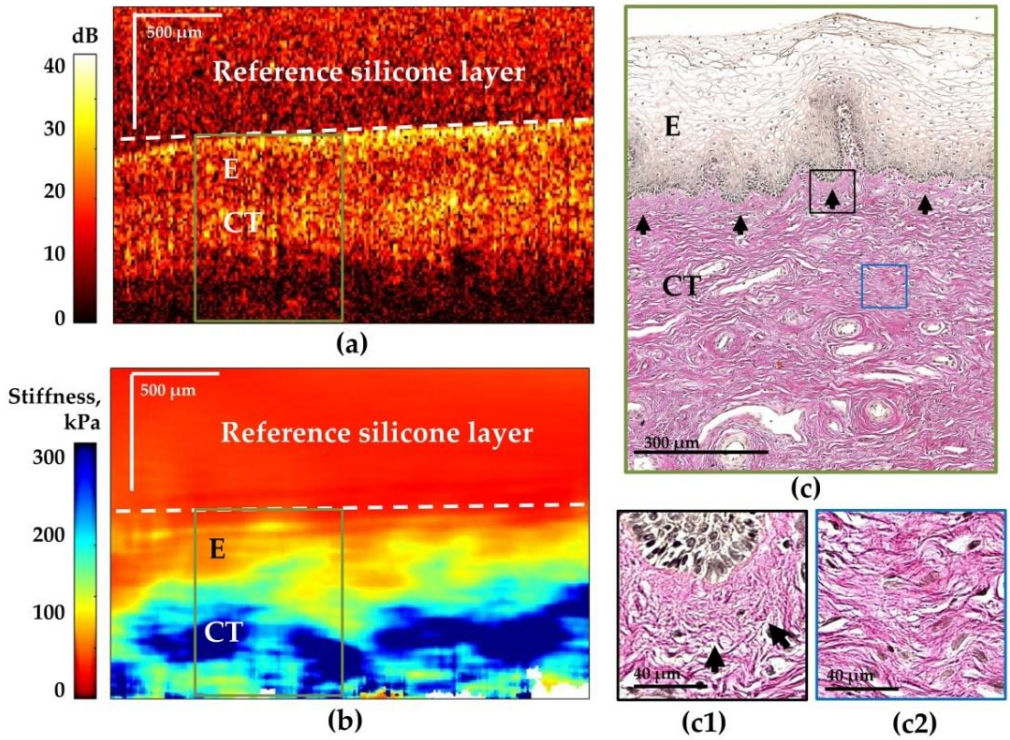

Figure 2. Representative depth-wise structural OCT (**a**) and C-OCE (**b**) images of age norm vaginal wall with the corresponding histology (**c**–**c2**). The right column (**c**–**c2**) is the histological slide stained with Van Gieson's, where (**c**)—an overview image of a well-organized two-layer tissue architecture with a sharp border between the glycogenated epithelium and the submucosal connective tissue underlying it, arrows indicate the subepithelial region of the stroma (×100); black square (**c1**)—subepithelial region of the submucosa, where black arrows point at very thin non-directional collagen bundles (×1000); and blue square (**c2**)—a deeper area of the submucosa, which is characterized by larger winding collagen fibers forming bundles and predominantly parallel to the epithelium, There are practically no spaces between them (×1000). White dotted lines on OCT (**a**) and C-OCE (**b**) images are the transition boundary between the calibration silicone layer and the tissue under study. The green box on the OCT (**a**) and C-OCE (**b**) images is the area corresponding to the histological image in (**c**). Abbreviations: E—epithelium, CT—connective tissue.

At the same time, the C-OCE image of the vaginal wall prolapse (Figure 3b) is mainly characterized by the significant lowest stiffness (72 ± 19 kPa) in the area of connective tissue in the subepithelial zone compared to age norm. Relatively high stiffness values (137 ± 21 kPa) were recorded only in the deeper submucosal zone (Figure 3b). This is consistent with histological images with the subepithelial zone characterized by very thin, loosely arranged collagen bundles (Figure 3c, arrows, and Figure 3(c1)). In the deeper layer of the submucosal connective tissue there are thin, but parallel to the epithelium, collagen bundles. At the same time, compared with age norm, collagen bundles are more organized, and enlarged slit-like spaces are observed between the bundles (Figure 3(c2)). This indicates that vaginal wall prolapse is characterized by a much softer and degenerated tissue structure than the dense, collagen-rich structure of the age norm.

It is worth noting that in the vaginal wall prolapse, due to the close stiffness values of the thinned epithelium (48 ± 11 kPa) and submucosal connective tissue in the subepithelial zone (72 ± 19 kPa), the boundary between these layers is not visualized as clearly (Figure 3b) as in the age norm (Figure 2b).

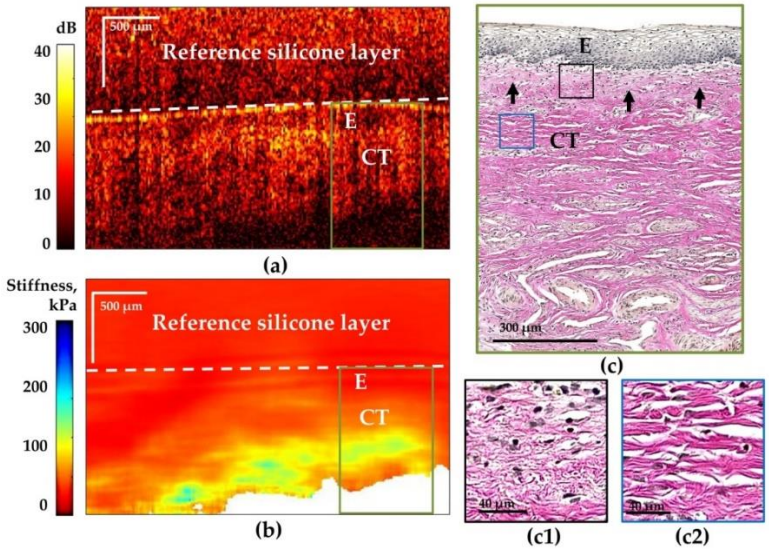

Figure 3. Representative depth-wise structural OCT (**a**) and C-OCE (**b**) images of stages I–II vaginal wall prolapse without preoperative treatment with the corresponding histology (**c**–**c2**). The right column (**c**,**c1**,**c2**) is the histological slide stained with Van Gieson's, where (**c**)—the overview image shows the subepithelial layer of loosely arranged collagen bundles (arrows) and a deeper layer with enlarged spaces between them, which indicates a decrease in the uniformity of their location (×100); black square (**c1**)—the area of the submucosal connective tissue with thin, loosely arranged collagen bundles (×1000); and blue square (**c2**)—deep area of the submucosal connective tissue with linear organized collagen bundles (×1000). The white dotted lines on OCT (**a**) and C-OCE (**b**) images are the transition boundary between the calibration silicone layer and the tissue under study. The green rectangle on OCT (**a**) and C-OCE (**b**) images is the area corresponding to the histological image on (**c**). Abbreviations: E—epithelium, CT—connective tissue.

The obtained results are consistent with the results of earlier studies suggesting a distinct decrease in the elastic modulus of tissues in POP compared to normal tissue [65,73]. However, in this study we demonstrate for the first time what specific changes in the collagen bundles of vaginal connective tissue are associated with a decrease in its elastic properties in the early stages of POP. The obtained results highlight a greater potential of the C-OCE method for assessing the condition of the submucosal connective tissue of the vaginal wall.

Figure 4 presents a common example of examination results of Nd:YAG laser-treated stages I–II vaginal wall prolapse. In the structural OCT (Figure 4a) and C-OCE (Figure 4b) images thickened epithelium is well visualized, with a low OCT signal level and low values stiffness (less than 100 kPa), respectively. This suggests normalization of epithelialization of the vaginal wall and the recovery of the glycogenized cell layer ((Figure 4c). Additionally, in the C-OCE image (Figure 4b), an uneven border between the epithelium and the submucosal connective tissue is clearly visualized. Histologically, this corresponds to visualized epithelial ridges that protrude into the subepithelial layer of the vaginal wall (Figure 4c).

The corresponding changes in the submucosal connective tissue were better visualized in the C-OCE image (Figure 4b) compared to the traditional structural OCT image (Figure 4a). A significant increase in the elastic modulus (142 ± 21 kPa) was found in the vaginal wall submucosal connective tissue in the C-OCE image (Figure 4b) compared with the vaginal wall prolapse without treatment (Figure 3b). Morphologically, tissue thickening occurs due to the formation of a dense network of thickened collagen bundles during the reorganization of connective tissue in response to laser treatment (Figure 4c). At the same time, it should be noted that according to histological examination, collagen bundles do not have a predominant direction; there is practically no space between them, which indicates an increase in the uniformity of their location (Figure 4(c1,c2)). There is no subepithelial layer of thin, intertwined collagen bundles (Figure 4(c1)).

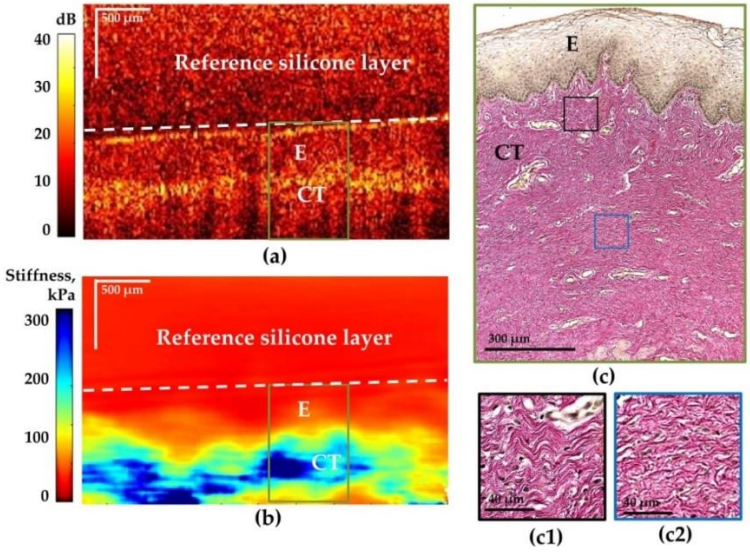

Figure 4. Representative depth-wise structural OCT (**a**) and C-OCE (**b**) images of stages I–II vaginal wall prolapse after Nd:YAG laser preoperative treatment and the corresponding histology (**c**–**c2**). The right column (**c**,**c1**,**c2**) is the histological slide stained with Van Gieson's, where (**c**)—the overview image shows a dense and homogeneous structure of the submucosal connective tissue without slit-like spaces (×100); the black square (**c1**)—the subepithelial region of the submucosal connective tissue consists of densely arranged collagen bundles (×1000); and the blue square (**c2**)—the deep area of the submucosal connective tissue, the tissue becomes even denser, and there are no spaces between the bundles (×1000). There is a well-organized two-layer architecture with a sharp interface between nonkeratinizing stratified squamous epithelium and underlying connective tissue. The white dotted lines in the OCT and C-OCE images are the boundary of the transition between the calibration silicone layer and the tissue under study. The green rectangle in the OCT and C-OCE images is the area corresponding to the histological image in (**c**). Abbreviations: E—epithelium, CT—connective tissue.

To conclude, we demonstrated that, firstly, C-OCE differentiates three states of vaginal connective tissues by the values of the elastic modulus: age norm, stages I–II prolapse and prolapse 1–2 months after the Nd:YAG laser therapy. Secondly, C-OCE images correlate well with the histological images. In the next "Section 3.2", progressing beyond the descriptive qualitative observations of Figures 2–4, we seek to quantify C-OCE and histological images in order to numerically distinguish between vaginal wall prolapse with and without laser preoperative treatment, as well as age norm.

3.2. Comparative Numerical Assessment of the C-OCE and Histological Images for Vaginal Wall at Different Conditions: Age Norm, Stages I–II Prolapse and Prolapse after Laser Treatment

For the first time in this study, textural quantitative analysis of histological images stained by Van Gieson was used to explain the relationship between elastic properties with the state of collagen fibers of the vaginal wall tissue in three studied groups (age norm, stages I–II prolapse and stages I–II prolapse post laser treatment).

Figure 5 demonstrates the general trend of stiffness value changes and collagen bundles structure parameters based on the quantitative assessment of C-OCE and histological images for each vaginal wall tissue condition studied.

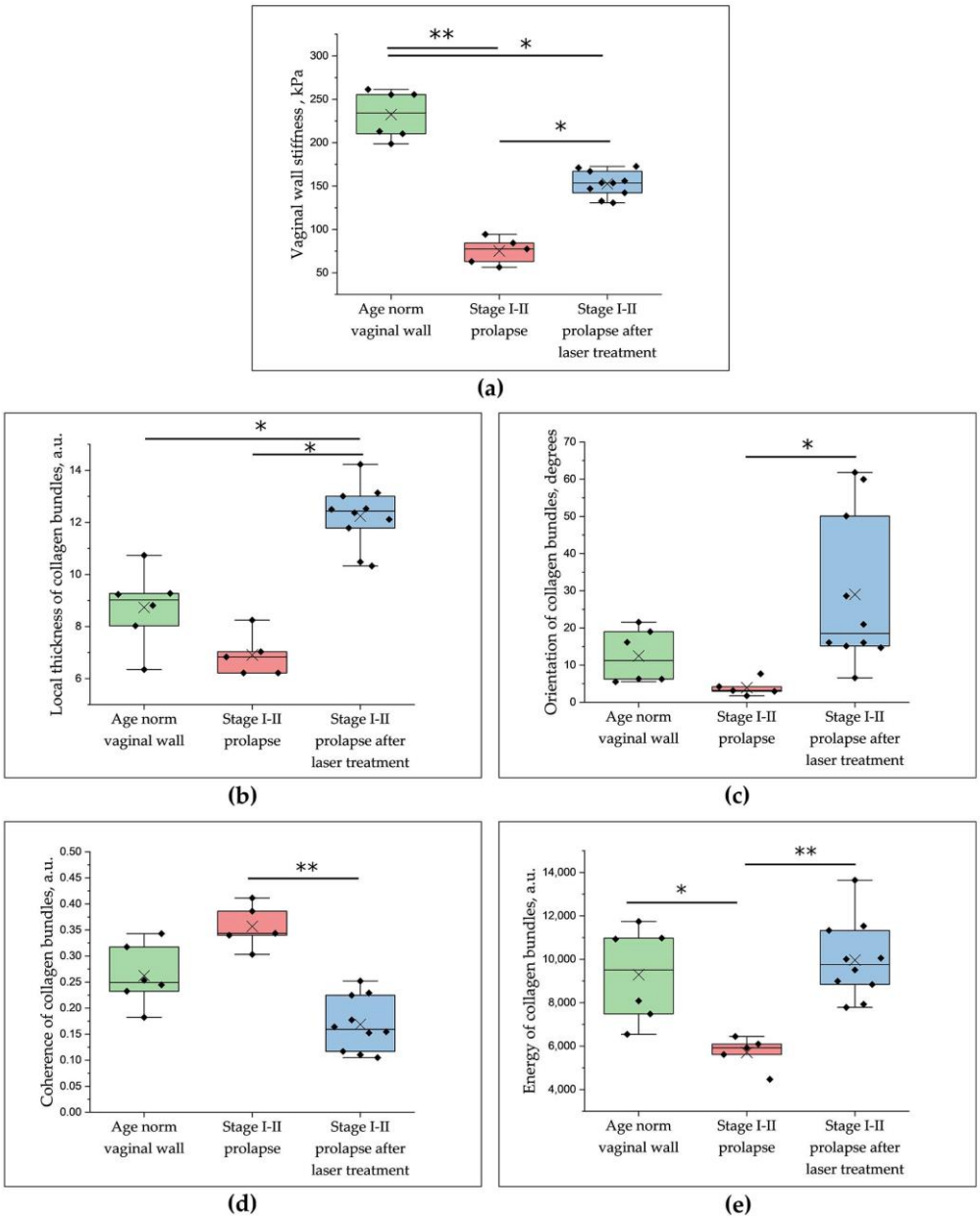

Figure 5. Quantitative assessment of C-OCE (**a**) and collagen bundles structure parameters (**b**–**e**) in three conditions of the vaginal wall: age norm, stage I–II prolapse and stage I–II prolapse after a course of Nd:YAG laser treatment. (**a**) Box plot of mean stiffness according to C-OCE data; (**b**) box plot local thickness of collagen bundles according to Van Gieson histological stain; (**c**) box plot orientation of collagen bundles according to Van Gieson histological stain (values are expressed modulo); (**d**) box plot organization (coherency) of collagen bundles according to Van Gieson histological stain; and (**e**) box plot uniformity (Energy) of collagen bundles according to Van Gieson histological stain. For each box plot, the center line represents medians, and "×" is the mean value of the analyzed parameter. Box plot limits indicate lower/upper quartiles (25th and 75th percentile), whiskers are minimum/maximum values within the 1.5× interquartile range of the first and third quartile, and notches are approximate 95% confidence intervals of the median. Segment indicates a statistically significant differences between the study groups, * and ** statistically significant ($p < 0.05$ and $p < 0.001$, respectively) (Mann–Whitney U test with Bonferroni correction). a.u.—arbitrary units.

Numerical assessment of the elasticity of the vaginal wall prolapse showed that the vaginal wall prolapse is characterized by a statistically significant decrease in average

stiffness compared to the age norm (73.5 ± 18.9 kPa vs. 233.5 ± 48.3 kPa, $p < 0.05$). It was found that in the vaginal wall prolapse, a decrease in stiffness (Figure 5a) is likely to be associated with a decrease in the local thickness of the collagen bundles (Figure 5b) and the energy parameter (Figure 5e), which indicates a violation of the uniformity of the arrangement of collagen bundles (Figure 4e) in the connective tissue of the vaginal wall. Additionally, in the vaginal wall prolapse, there is a decrease in the orientation (angle of inclination) of the location of the collagen bundles relative to the epithelium and an increase in the coherence parameter (Figure 5d), which indicates a more dominant (organized) direction of the location of the collagen bundles compared to the age norm. At the same time, the energy parameter reflecting the uniformity of the location of collagen bundles in the vaginal wall tissue turned out to be the only statistically significant parameter distinguishing the submucosal connective tissue in age norm and in the early stage of vaginal wall prolapse (8728 ± 2827 a.u. vs. 5746 ± 944 a.u.; $p < 0.05$) (Figure 5e). The decrease in energy during vaginal wall prolapse is likely to be associated with an increase in the spaces between the bundles of collagen fibers (Figure 4(c2)), which naturally leads to an increase in tissue heterogeneity.

After the laser treatment, the vaginal connective tissue is characterized by a statistically significant increase in the average stiffness value relative to the group of patients with early stage of vaginal wall prolapse (152.1 ± 19.2 kPa vs. 73.5 ± 18.9 kPa; $p < 0.05$) (Figure 5a). The increase in tissue stiffness after laser treatment is most likely due to an increase in the local thickness of the collagen bundles, as well as the energy parameter, indicating an increase in the uniformity of the arrangement of the collagen bundles. We demonstrate that under laser exposure, the submucosal connective tissue of the vaginal wall is characterized by a statistically significant increase in the local thickness of collagen bundles in relation to both groups, with an early stage of vaginal wall prolapse and age norm (12.2 ± 1.2 a.u. vs. 7 ± 1.3 a.u. and 12.2 ± 1.2 a.u. vs. 8.7 ± 1.4 a.u.; $p < 0.05$) (Figure 4a). However, this does not indicate a real increase in the thickness of the collagen bundles. It can be assumed that the increase in local thickness is due to a change in orientation (Figure 5c) and an increase in the uniformity (energy) of the beam arrangement (Figure 5e). This leads to the groups of collagen bundles being recognized by the "LocalThickness" plugin as a single structural element. It is worth noting that the values of the energy and coherence parameters of the collagen bundles after laser exposure reach the range of values characteristic of the age norm vaginal wall (Figure 5c,d). A change in orientation in the group with laser exposure relative to the group with vaginal wall prolapse is accompanied by a decrease in the coherence of the collagen bundles, which means that they lose their dominant direction (Figure 4(c2)). In the group with laser exposure in relation to the group with an early stage of vaginal wall prolapse, there is also a statistically significant increase in the values of the energy parameter and a decrease in the coherence parameter (9960 ± 1799 a.u. vs. 5746 ± 944 a.u. and 0.17 ± 0.05 a.u. vs. 0.26 ± 0.06 a.u.; $p < 0.05$).

The performed C-OCE examination and analysis of the complementary histological images indicate that the stiffness values are affected by the local thickness, density and heterogeneity of the collagen bundles. In particular, the stiffness reduction is observed when the collagen bundles become thinner and less densely packed and demonstrate a fairly clear dominant direction. The stiffness increase is associated with larger thickness of collagen bundles when they are more densely packed and lose their dominant direction.

In order to analyze the relation between stiffness according to C-OCE data and collagen bundles, structure parameters according to histology data of the Spearman's correlation coefficient were calculated (Figure 6). The correlation analysis identified three pairs of correlated parameters only in the vaginal wall prolapse without and after laser treatment. There was a high positive correlation between the vaginal wall stiffness and the local thickness of the collagen bundles, as well as with the energy parameter of the collagen bundles ($r = 0.668$, $p = 0.006$; $r = 0.714$, $p = 0.003$) (Figure 6a,c). At the same time, the stiffness demonstrated negative correlation with the coherence parameter ($r = -0.568$; $p = 0.027$) (Figure 6b). Thus, this fairly high correlation indicates that the vaginal wall

stiffness visualized by C-OCE with the resolution corresponding to the scales of tissue organization is affected by the structural characteristics of the collagen bundles.

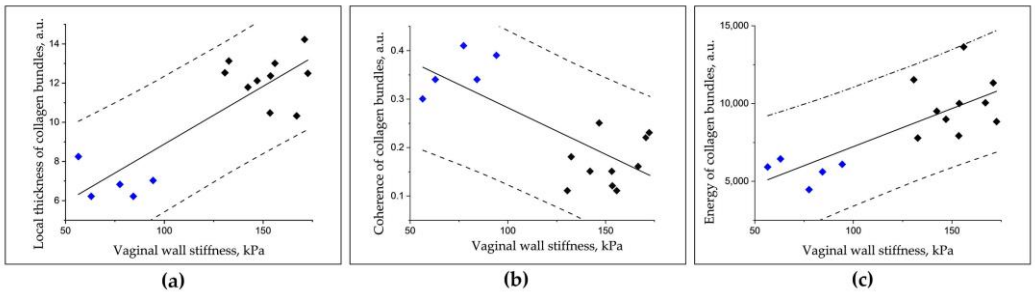

Figure 6. Relation between stiffness according to C-OCE data and collagen bundles structure parameters according to histology data in the vaginal wall with stage I–II prolapse (blue squares) and stage I–II prolapse after a course of Nd:YAG laser treatment (black squares). (**a**) High positive correlation is demonstrated between vaginal wall stiffness and local thickness of the collagen bundles (r = 0.668, $p = 0.006$). (**b**) An inverse relationship is demonstrated between vaginal wall stiffness and coherence parameter of the collagen bundles (r = −0.568, $p = 0.027$). (**c**) High positive correlation is demonstrated between vaginal wall stiffness and the energy parameter of the collagen bundles (r = 0.714, $p = 0.003$). The dotted lines show 95% prediction intervals.

Thus, the results of a comparative numerical analysis of C-OCE and histological images showed that with vaginal wall prolapse, the main focus of quantitative changes in the submucosal connective tissue of the vaginal wall, reflects the development of destructive processes. This is expressed in a decrease in stiffness values based on a quantitative assessment of C-OCE images and the uniformity of the arrangement of collagen bundles based on a quantitative assessment of histological images. On the contrary, the nature of the reorganization of the vaginal wall tissues after Nd:YAG laser exposure is determined by an increase in the quantitative indicators of the connective tissue structures of the vaginal wall submucosal connective tissue in histological images and the restoration of elastic modulus in C-OCE images, which indicate an intensification of regenerative reactions and an improvement in the morphometric parameters of the tissue.

4. Discussion

In this paper, for the first time, we applied C-OCE technique for a comparative assessment of changes in the elasticity of the vaginal wall tissue in different conditions: age norm, stage I–II prolapse, and stage I–II prolapse after Nd:YAG laser treatment. The previous applications of the C-OCE method by our and other research groups mainly related to the field of oncology. In those studies, the high potential of OCE was shown to differentiate benign and malignant tumors, such as prostate cancer [74], breast cancer [50,51], and ovarian cancer [54], by absolute stiffness values. However, there are very few publications in the world literature on the application of the OCE for assessing the elastic modulus in non-tumor processes, particularly in the field of gynecology.

The use of C-OCE to assess the absolute stiffness values of the vaginal wall in prolapse may have high potential due to objective elasticity changes of the vaginal connective tissue. It is known that the predominant pathogenetic mechanism of POP is the decreased synthesis and the increased breakdown of the extracellular matrix in the connective tissue of the pelvic floor, with collagen being its main component [75]. Numerous mechanisms are responsible for the disruption in the balanced collagen metabolism. Decreased estrogen secretion, genetic predisposition, and oxidative stress can lead to a decrease in collagen synthesis, activation of matrix metalloproteinases responsible for collagen degradation, as well as changes in the amino acid sequence in procollagen chains. These processes lead to a decrease in the biomechanical strength of the supporting connective tissues of the pelvis. It is worth noting that early stages of vaginal wall prolapse are usually not

easily detected on ultrasound or by direct visualization using colposcopy. This is caused by the insufficient resolution of those methods to visualize the initial changes of elasticity in the connective tissue of the vaginal wall just below the epithelium. Up to now, the histological examination of biopsy samples remains the gold standard in the evaluation of connective tissue in gynecology. However, such examinations are rather time consuming and laborious. In comparison with such conventional techniques used in gynecology, modern optical imaging methods have important advantages. Thus, the OCT method used in this study is a non-invasive optical analog to ultrasound with significantly higher resolution (4–10 μm), and a penetration depth of ~2 mm, enabling three-dimensional high-speed imaging (nowadays, hundreds of frames per second are possible). The size of OCT images is comparable with conventional histological images. Furthermore, the emerging OCT-based modalities, such as OCE and possibilities of objective quantitative analysis of the OCT data in combination with real-time imaging, additionally extend the variety of clinical applications of OCT methods. In an earlier study, our group tested the application of C-OCE technology to evaluate the vaginal wall state using postoperative samples of patients with stage IV prolapse [65]. In this pilot study, we demonstrated significant differences not only in the values of Young's modulus, but also in the character of elastic responses in age norm vaginal wall and stage IV prolapse. Here, we demonstrated that stiffness of vaginal wall prolapse is significantly decreased and slightly varied with compression, which clearly suggests the decrease in biomechanical properties of the vaginal wall. The results of the current study on stage I–II prolapse are in full agreement with our previous results. Moreover, a comparative analysis of C-OCE numerical evaluation data and histological images was used for the first time for objective data analysis. The main clinical value of this study is demonstrating the ability of C-OCE to detect early stages of prolapse using reduced stiffness values compared to the age norm of the vaginal wall. As it was shown based on the analysis of histological data, significant decreases in the stiffness value are due to a decrease in the uniformity and density of the location of collagen bundles in the vaginal walls in patients with stage I–II prolapse compared with the age norm vaginal wall. This confirmed that C-OCE imaging looks very promising for detection of early stages of vaginal wall prolapse, with much higher contrast than, for example, conventional structural OCT images. The structural OCT image of the vaginal wall prolapse reflected only a decrease in the thickness of the epithelium and did not reflect the true state of the submucosal connective tissue (Figure 3a). Our results on assessing elasticity changes of the vaginal wall are also consistent with the data on the quantifying vaginal tissue elastic modulus under normal and prolapse conditions by vaginal tactile imaging based on principles similar to those of manual palpation [73].

It is important to note that the histological diagnosis of POP based on an assessment of the condition of the vaginal wall submucosal connective tissue remains an unsolved problem because histological changes in women with POP are inconclusive and relatively limited [76]. Histological and immunohistochemical studies of collagen bundles have contradictory results. Some studies identify molecular disorganization and fragmentation of collagen fibers [77] and reduction in the immuno-staining of type I, III, and V collagen in the vaginal wall [78]. Others report an increase in the number of collagen fibers and a decrease in the number of fibroblasts in POP [79], as well as an increase in the expression of type III collagen [80]. Therefore, there are no uniform ideas about the change in collagen bundles in POP [76].

Currently, three different laser modalities for treating gynecological and urological problems (genitourinary syndrome, dilated vagina syndrome, and stress urinary incontinence) and for vaginal rejuvenation were reported on: (1) microablative fractional carbon di-oxide (CO_2) laser therapy (10,600 nm) [20–22]; (2) dual-phase erbium-doped yttrium aluminium garnet (Er:YAG) laser therapy (2940 nm) combining fractional cold ablation and thermal ablation [23,24]; and non-ablative Er:YAG laser therapy (2940 nm) with SMOOTH mode technology [25,26]. In all three cases, laser therapy induces neocollagenesis, as well as thickens and strengthens the anterior vaginal wall, which leads to improved support of

the bladder and urethra [22]. For the first time, we used the C-OCE method to assess the elastic modulus increase in the vaginal wall after laser therapy. Additionally, for the first time, a neodymium non-ablative laser was used in treatment of stages I–II prolapse. The advantage of this laser is non-invasive exposure, absence of complications, and reduction in the rehabilitation period to 1 week instead of 1 month after ablative laser exposure. In addition, due to the low absorption of the main components of the tissue (water and collagen), the effect is carried out on the entire depth of the mucosa, including its own plate, while classical ablation lasers create micro-damage only in the surface layer at the depth of several microns. Thus, neodymium non-ablative laser treatment of the POP can compete with conservative methods [81–83], physiotherapeutic techniques [84] traditionally used in the clinic today, as well as microablative laser therapy approaches that are being developed today. At the same time, surgical correction remains the main method of treatment of POP, with more than 30% of relapses being recorded [3].

In this study, we demonstrate that C-OCE images of vaginal wall tissue samples in patients with stage I–II prolapse 1–2 months after the use of Nd:YAG laser radiation treatment had significant differences compared to C-OCE images of vaginal wall samples in patients with stage I–II prolapse without treatment. In contrast to vaginal wall prolapse samples, the connective tissue of the vaginal wall after laser treatment on C-OCE images in most cases was characterized by a significant increase in the tissue stiffness. As it was shown based on the analysis of histological data, this was due to an increase in the local thickness of the collagen bundles due to a change in their orientation and an increase in the uniformity of their location (see Figure 5) with minimal slit-like spaces between them. It is worth noting that quantitative textural analysis of collagen bundles based on histological images stained according to Van Gieson with the aim to substantiate the elastic properties of the vaginal wall was used for the first time. Earlier, textural analysis of histological images was used to study the organization of collagen bundles in scars [85], classification of histological images of breast cancer [86], and to find a connection between textural features of the image and the parameters of polarization of invasive ductal carcinoma tissue [87]. In this study, a similar approach was used to analyze the overall structure and organization of specifically colored collagen bundles to reveal the connection with the variations in the elastic modulus of the vaginal wall.

The performed study demonstrated rather high and statistically significant correlation coefficients characterizing the relation of the elastic modulus evaluated using C-OCE images, with the parameters of the local thickness, as well as coherence and energy of collagen fibers estimated using histological images ($r = 0.668$, $r = -0.568$ and $r = 0.714$; $p < 0.05$; respectively) for the early stage of vaginal wall prolapse without treatment and after laser treatment. This allows one to utilize C-OCE images for estimating the structural organization of the collagen bundles in the connective tissue. We hypothesize that the not-so-high values of the correlation coefficients are related to the rather limited amount of data. It may be expected that a study utilizing data from a larger number of patients would demonstrate a higher correlation level among the analyzed parameters extracted from the C-OCE and histological images.

It can be noted that much attention in biophotonics is paid to various ways of increasing resolution of optical diagnostics methods, including utilization of nonlinear optical and even quantum optical effects to achieve nano-scale super resolution beyond the diffraction limit [88]. In this context, it should be emphasized that although the resolution of the C-OCE technique (~several tens of micrometers) is significantly higher than for conventional ultrasound elastography, at the same time, it is much lower in comparison with the sub-cellular probing of elasticity enabled by atomic force microscopy. However, it should be emphasized that sub-cellular resolution is too high when there is a need to study the elasticity on a scale characterizing the organization of morphological components of tissues, i.e., from several tens to a few hundred micrometers. Thus, the “mesoscale” resolution enabled by C-OCE perfectly corresponds to such applications. In the above examples, the changes in the structural organization of the collagen bundles were not directly resolved in

C-OCE. Nevertheless, manifestations of these structural changes were perfectly observed in our study through the visualized variations in the tissue elasticity.

It is also worth noting that using the C-OCE method, we were able to show that elastic properties of the vaginal wall tissue after laser exposure do not recover to the normal range of stiffness values, despite the fact that quantitative histological data demonstrate the restoration of the studied parameters. This can be explained by the fact that collagen bundles are not the only structural elements of the submucosal connective tissue responsible for the elasticity of the tissue. Elastic fibers also have a significant effect on the stiffness of the vaginal wall [89]; however, they were not studied in this pilot work. Moreover, it is also possible to hypothesize that not enough time passed (no more than 2 months) to allow full restoration of the elastic properties. Therefore, we intend to conduct further research on a larger number of patients, with expanded histological analysis of data, and clinical and OCT monitoring being carried out 6 and 12 months after laser therapy, which will allow us to assess the efficacy and duration of the effect of laser exposure depending on the age and other patient characteristics. In the future, we anticipate that repeated laser therapy courses could be carried out to prevent a relapse of POP. The use of C-OCE could eliminate the need for invasive (puncture biopsy) manipulations in patients for morphological and immunohistochemical analysis before or after laser treatment. In addition, C-OCE can be applied to tissue discrimination as a kind of "optical biopsy" for aiding diagnosis, assess the efficacy of treatment, or even for guide biopsy sample harvesting in clinical examination or surgeries in various organs.

Our findings demonstrate a significant potential of the imaging approach to examining the vaginal wall structure using C-OCE that could serve as a basis for future in vivo clinical studies. However, despite these promising results, it is also possible to foresee that the most likely obstacle to the OCT application in gynecology in real clinical conditions would be the need for an OCT probe of certain geometry, as well as the need for a correct interpretation of the obtained OCT and C-OCE image data by a gynecologist in order to exclude the possibility of an incorrect diagnosis. To address the latter challenge, automatic numerical image processing would be essential to improve the diagnostic accuracy of OCT. Our future research aims to target this task.

5. Conclusions

The results of this pilot study demonstrate that C-OCE can provide real-time and high-resolution imaging to view vaginal wall structure with high consistency with histological examination. C-OCE is capable of assessing the condition of collagen bundles in the vaginal wall submucosal connective tissue objectively and accurately, thus holding promise as a potential tool for earlier identification of vaginal wall prolapse in vivo and monitoring laser treatment efficiency in future studies. This type of technology is missing in the field of pelvic medicine today and has great potential. As we work to increase the accuracy of this technology, we believe that it will become a valuable tool for monitoring treatment response, contributing to individual treatment plans, and a potential guidance tool for surgeons during minimally invasive surgery.

Author Contributions: Conceptualization, G.G., K.S., N.G. and M.S.; images analysis, E.G., A.P. and D.K.; C-OCE method development and software for OCE-visualization, A.S. and V.Z.; histological analysis, A.P., S.R.-L. and M.K.; data curation, D.K., K.S. and A.K.; writing—original draft preparation, E.G. and A.P.; writing—review and editing, M.S., G.G., S.R.-L., N.G., V.Z. and K.S.; visualization, E.G., A.P. and M.L.; clinical work, D.K.; supervision, K.S., A.K. and M.S. All authors have read and agreed to the published version of the manuscript.

Funding: Development of the diagnostic approach to elastic evaluation of vaginal wall tissue using C-OCE was supported by Center of Excellence "Center of Photonics" funded by The Ministry of Science and Higher Education of the Russian Federation, contract No 075-15-2020-927.

Institutional Review Board Statement: This study was approved by the Institutional Review Board of the Privolzhsky Research Medical University (Protocol #13 from 7 July 2021, protocol #2 from 4 February 2022).

Informed Consent Statement: Informed consent was obtained from all subjects involved in the study. Written informed consent has been obtained from the patients to publish data in scientific literature.

Data Availability Statement: The data presented in this study are available on request from the corresponding author. The data are not publicly available due to proprietary rules.

Acknowledgments: The authors thank to "MeLSyTech", Ltd. for technical support of the study and support in histological studies.

Conflicts of Interest: D.K. is a researcher on clinical study and receives payments from "MeLSyTech", Ltd. G.G. is the lead researcher on clinical study and receives consulting payments from "MeLSyTech", Ltd. K.S. and A.K. are researchers on this study and receive a regular salary from "MeLSyTech", Ltd. as employees. All other authors declare no conflict of interest.

References

1. Abhyankar, P.; Uny, I.; Semple, K.; Wane, S.; Hagen, S.; Wilkinson, J.; Guerrero, K.; Tincello, D.; Duncan, E.; Calveley, E.; et al. Women's Experiences of Receiving Care for Pelvic Organ Prolapse: A Qualitative Study. *BMC Women's Health* **2019**, *19*, 45. [CrossRef]
2. Hallock, J.L.; Handa, V.L. The Epidemiology of Pelvic Floor Disorders and Childbirth. *Obstet. Gynecol. Clin. N. Am.* **2016**, *43*, 1–13. [CrossRef] [PubMed]
3. Vergeldt, T.F.M.; Weemhoff, M.; IntHout, J.; Kluivers, K.B. Risk Factors for Pelvic Organ Prolapse and Its Recurrence: A Systematic Review. *Int. Urogynecol. J.* **2015**, *26*, 1559–1573. [CrossRef] [PubMed]
4. Weintraub, A.Y.; Glinter, H.; Marcus-Braun, N. Narrative Review of the Epidemiology, Diagnosis and Pathophysiology of Pelvic Organ Prolapse. *Int. Braz. J. Urol.* **2020**, *46*, 5–14. [CrossRef] [PubMed]
5. Iglesia, C.B.; Smithling, K.R. Pelvic Organ Prolapse. *Am. Fam. Physician* **2017**, *96*, 179–185.
6. Abramowitch, S.D.; Feola, A.; Jallah, Z.; Moalli, P.A. Tissue Mechanics, Animal Models, and Pelvic Organ Prolapse: A Review. *Eur. J. Obstet. Gynecol. Reprod. Biol.* **2009**, *144*, S146–S158. [CrossRef] [PubMed]
7. Jean-Charles, C.; Rubod, C.; Brieu, M.; Boukerrou, M.; Fasel, J.; Cosson, M. Biomechanical Properties of Prolapsed or Non-Prolapsed Vaginal Tissue: Impact on Genital Prolapse Surgery. *Int. Urogynecol. J.* **2010**, *21*, 1535–1538. [CrossRef]
8. Ophir, J. Elastography: A Quantitative Method for Imaging the Elasticity of Biological Tissues. *Ultrason. Imaging* **1991**, *13*, 111–134. [CrossRef]
9. Manduca, A.; Oliphant, T.E.; Dresner, M.A.; Mahowald, J.L.; Kruse, S.A.; Amromin, E.; Felmlee, J.P.; Greenleaf, J.F.; Ehman, R.L. Magnetic Resonance Elastography: Non-Invasive Mapping of Tissue Elasticity. *Med. Image Anal.* **2001**, *5*, 237–254. [CrossRef]
10. Nanjappa, M.; Kolipaka, A. Magnetic Resonance Elastography of the Brain. *Magn. Reson. Imaging Clin. N. Am.* **2021**, *29*, 617–630. [CrossRef]
11. Wang, J.; Deng, Y.; Jondal, D.; Woodrum, D.M.; Shi, Y.; Yin, M.; Venkatesh, S.K. New and Emerging Applications of Magnetic Resonance Elastography of Other Abdominal Organs. *Top. Magn. Reson. Imaging* **2018**, *27*, 335–352. [CrossRef] [PubMed]
12. Sigrist, R.M.S.; Liau, J.; Kaffas, A.E.; Chammas, M.C.; Willmann, J.K. Ultrasound Elastography: Review of Techniques and Clinical Applications. *Theranostics* **2017**, *7*, 1303–1329. [CrossRef] [PubMed]
13. Morris, D.C.; Chan, D.Y.; Palmeri, M.L.; Polascik, T.J.; Foo, W.-C.; Nightingale, K.R. Prostate Cancer Detection Using 3-D Shear Wave Elasticity Imaging. *Ultrasound Med. Biol.* **2021**, *47*, 1670–1680. [CrossRef] [PubMed]
14. Huang, D.; Swanson, E.A.; Lin, C.P.; Schuman, J.S.; Stinson, W.G.; Chang, W.; Hee, M.R.; Flotte, T.; Gregory, K.; Puliafito, C.A.; et al. Optical Coherence Tomography. *Science* **1991**, *254*, 1178–1181. [CrossRef] [PubMed]
15. Drexler, W.; Liu, M.; Kumar, A.; Kamali, T.; Unterhuber, A.; Leitgeb, R.A. Optical Coherence Tomography Today: Speed, Contrast, and Multimodality. *J. Biomed. Opt.* **2014**, *19*, 071412. [CrossRef] [PubMed]
16. Leitgeb, R.; Placzek, F.; Rank, E.; Krainz, L.; Haindl, R.; Li, Q.; Liu, M.; Andreana, M.; Unterhuber, A.; Schmoll, T.; et al. Enhanced Medical Diagnosis for DOCTors: A Perspective of Optical Coherence Tomography. *J. Biomed. Opt.* **2021**, 26. [CrossRef]
17. Cogliati, A.; Canavesi, C.; Hayes, A.; Tankam, P.; Duma, V.-F.; Santhanam, A.; Thompson, K.P.; Rolland, J.P. MEMS-Based Handheld Scanning Probe with Pre-Shaped Input Signals for Distortion-Free Images in Gabor-Domain Optical Coherence Microscopy. *Opt. Express* **2016**, *24*, 13365. [CrossRef]
18. Loran, O.B.; Seregin, A.S.; Dovlatov, Z.A. The clinical outcomes of the modern minimally invasive technologies in the treatment of the female pelvic organ prolaps. *Eksperimental'naya I Klin. Urol.* **2015**, *2*, 124–130.
19. Baessler, K.; Christmann-Schmid, C.; Maher, C.; Haya, N.; Crawford, T.J.; Brown, J. Surgery for Women with Pelvic Organ Prolapse with or without Stress Urinary Incontinence. *Cochrane Database Syst. Rev.* **2018**, 2018. [CrossRef]
20. González Isaza, P.; Jaguszewska, K.; Cardona, J.L.; Lukaszuk, M. Long-Term Effect of Thermoablative Fractional CO_2 Laser Treatment as a Novel Approach to Urinary Incontinence Management in Women with Genitourinary Syndrome of Menopause. *Int. Urogynecol. J.* **2018**, *29*, 211–215. [CrossRef]

21. Paraiso, M.F.R.; Ferrando, C.A.; Sokol, E.R.; Rardin, C.R.; Matthews, C.A.; Karram, M.M.; Iglesia, C.B. A Randomized Clinical Trial Comparing Vaginal Laser Therapy to Vaginal Estrogen Therapy in Women with Genitourinary Syndrome of Menopause: The VeLVET Trial. *Menopause* **2020**, *27*, 50–56. [CrossRef] [PubMed]
22. Salvatore, S.; Leone Roberti Maggiore, U.; Athanasiou, S.; Origoni, M.; Candiani, M.; Calligaro, A.; Zerbinati, N. Histological Study on the Effects of Microablative Fractional CO_2 Laser on Atrophic Vaginal Tissue: An Ex Vivo Study. *Menopause* **2015**, *22*, 845–849. [CrossRef] [PubMed]
23. Mothes, A.R.; Runnebaum, M.; Runnebaum, I.B. An Innovative Dual-Phase Protocol for Pulsed Ablative Vaginal Erbium:YAG Laser Treatment of Urogynecological Symptoms. *Eur. J. Obstet. Gynecol. Reprod. Biol.* **2018**, *229*, 167–171. [CrossRef] [PubMed]
24. Gambacciani, M.; Palacios, S. Laser Therapy for the Restoration of Vaginal Function. *Maturitas* **2017**, *99*, 10–15. [CrossRef] [PubMed]
25. Lukac, M.; Gaspar, A.; Bajd, F. Dual tissue regeneration: Non-ablative resurfacing of soft tissues with FotonaSmooth® mode Er:YAG laser. *J. Laser Health Acad.* **2018**, *1*, 1–15.
26. Fistonić, N.; Fistonić, I.; Guštek, Š.F.; Turina, I.S.B.; Marton, I.; Vižintin, Z.; Kažič, M.; Hreljac, I.; Perhavec, T.; Lukač, M. Minimally Invasive, Non-Ablative Er:YAG Laser Treatment of Stress Urinary Incontinence in Women—a Pilot Study. *Lasers Med. Sci.* **2016**, *31*, 635–643. [CrossRef]
27. Gaspar, A.; Brandi, H.; Gomez, V.; Luque, D. Efficacy of Erbium:YAG Laser Treatment Compared to Topical Estriol Treatment for Symptoms of Genitourinary Syndrome of Menopause: EFFICACY OF ERBIUM:YAG LASER TREATMENT OF GSM. *Lasers Surg. Med.* **2017**, *49*, 160–168. [CrossRef]
28. Ishchenko, A.A.; Ishchenko, A.I.; Shulchina, I.V.; Muravlev, A.I. Use of Laser Technologies in a Complex of Arrangements to Patients Operated for the Genital Prolapse. *GYN* **2016**, *18*. [CrossRef]
29. Vogel, A.; Venugopalan, V. Mechanisms of Pulsed Laser Ablation of Biological Tissues. *Chem. Rev.* **2003**, *103*, 577–644. [CrossRef]
30. Jacques, S.L. Optical Properties of Biological Tissues: A Review. *Phys. Med. Biol.* **2013**, *58*, R37–R61. [CrossRef]
31. Taroni, P.; Comelli, D.; Pifferi, A.; Torricelli, A.; Cubeddu, R. Absorption of Collagen: Effects on the Estimate of Breast Composition and Related Diagnostic Implications. *J. Biomed. Opt.* **2007**, *12*, 014021. [CrossRef] [PubMed]
32. Sajjadi, A.Y.; Mitra, K.; Grace, M. Expression of Heat Shock Proteins 70 and 47 in Tissues Following Short-Pulse Laser Irradiation: Assessment of Thermal Damage and Healing. *Med. Eng. Phys.* **2013**, *35*, 1406–1414. [CrossRef] [PubMed]
33. Souil, E.; Capon, A.; Mordon, S.; Dinh-Xuan, A.T.; Polla, B.S.; Bachelet, M. Treatment with 815-Nm Diode Laser Induces Long-Lasting Expression of 72-KDa Heat Shock Protein in Normal Rat Skin. *Br. J. Dermatol.* **2001**, *144*, 260–266. [CrossRef]
34. Goldberg, D.J.; Silapunt, S. Histologic Evaluation of a Q-Switched Nd:YAG Laser in the Nonablative Treatment of Wrinkles. *Dermatol. Surg.* **2001**, *27*, 744–746. [CrossRef] [PubMed]
35. Kulikov, I.A.; Apolikhina, I.A.; Spokoinyi, L.B. Vozmozhnosti primeneniia neodimovogo lazera (ND:YAG) v ginekologii. *Metamorfozy* **2019**, *26*, 26–31. (In Russian)
36. Pauzina, O.A.; Apolikhina, I.A. Vozmozhnosti primeneniya neodimovogo lazera (ND:YAG) v ginekologicheskoy praktike. *GLAVVRACH* **2020**, 6. (In Russian) [CrossRef]
37. Pauzina, O.A.; Apolikhina, I.A.; Malyshkina, D.A. Possibilities of using neodymium laser (Nd:YAG) in patients with concomitant diseases which are accompanied by pathological discharge from the genital tract. *Gynecology* **2020**, *22*, 75–81. [CrossRef]
38. Vincent, K.L.; Stanberry, L.R.; Moench, T.R.; Breitkopf, C.R.; Loza, M.L.; Wei, J.; Grady, J.; Paull, J.; Motamedi, M.; Rosenthal, S.L. Optical Coherence Tomography Compared With Colposcopy for Assessment of Vaginal Epithelial Damage: A Randomized Controlled Trial. *Obstet. Gynecol.* **2011**, *118*, 1354–1361. [CrossRef]
39. Shalom, D.F.; Ledford, K.J.; Qadir, A.; Lind, L.R.; Winkler, H.A. Visualization of Synthetic Mesh Utilizing Optical Coherence Tomography. *Int. Urogynecol. J.* **2013**, *24*, 1909–1914. [CrossRef]
40. Nandy, S.; Sanders, M.; Zhu, Q. Classification and Analysis of Human Ovarian Tissue Using Full Field Optical Coherence Tomography. *Biomed. Opt. Express* **2016**, *7*, 5182. [CrossRef]
41. Yang, Y.; Wang, T.; Biswal, N.C.; Wang, X.; Sanders, M.; Brewer, M.; Zhu, Q. Optical Scattering Coefficient Estimated by Optical Coherence Tomography Correlates with Collagen Content in Ovarian Tissue. *J. Biomed. Opt.* **2011**, *16*, 090504. [CrossRef] [PubMed]
42. Hariri, L.P.; Bonnema, G.T.; Schmidt, K.; Winkler, A.M.; Korde, V.; Hatch, K.D.; Davis, J.R.; Brewer, M.A.; Barton, J.K. Laparoscopic Optical Coherence Tomography Imaging of Human Ovarian Cancer. *Gynecol. Oncol.* **2009**, *114*, 188–194. [CrossRef] [PubMed]
43. Sudol, N.T.; Miao, Y.; Li, Y.; Chen, J.J.; Jing, J.C.; Zhu, J.; Tadir, Y.; Chen, Z.; Lane, F. Optical Vaginal Biopsy Using Optical Coherence Tomography. *Female Pelvic. Med. Reconstr. Surg.* **2020**, *26*, 155–158. [CrossRef] [PubMed]
44. Gubarkova, E.V.; Kiseleva, E.B.; Sirotkina, M.A.; Vorontsov, D.A.; Achkasova, K.A.; Kuznetsov, S.S.; Yashin, K.S.; Matveyev, A.L.; Sovetsky, A.A.; Matveev, L.A.; et al. Diagnostic Accuracy of Cross-Polarization OCT and OCT-Elastography for Differentiation of Breast Cancer Subtypes: Comparative Study. *Diagnostics* **2020**, *10*, 994. [CrossRef] [PubMed]
45. Schmitt, J.M. OCT Elastography: Imaging Microscopic Deformation and Strain of Tissue. *Opt. Express* **1998**, *3*, 199. [CrossRef]
46. Zaitsev, V.Y.; Matveyev, A.L.; Matveev, L.A.; Sovetsky, A.A.; Hepburn, M.S.; Mowla, A.; Kennedy, B.F. Strain and Elasticity Imaging in Compression Optical Coherence Elastography: The Two-decade Perspective and Recent Advances. *J. Biophotonics* **2021**, *14*, e202000257. [CrossRef]
47. Larin, K.V.; Sampson, D.D. Optical Coherence Elastography – OCT at Work in Tissue Biomechanics [Invited]. *Biomed. Opt. Express* **2017**, *8*, 1172. [CrossRef]

48. Li, E.; Makita, S.; Azuma, S.; Miyazawa, A.; Yasuno, Y. Compression Optical Coherence Elastography with Two-Dimensional Displacement Measurement and Local Deformation Visualization. *Opt. Lett.* **2019**, *44*, 787. [CrossRef]
49. Kennedy, K.M.; Zilkens, R.; Allen, W.M.; Foo, K.Y.; Fang, Q.; Chin, L.; Sanderson, R.W.; Anstie, J.; Wijesinghe, P.; Curatolo, A.; et al. Diagnostic Accuracy of Quantitative Micro-Elastography for Margin Assessment in Breast-Conserving Surgery. *Cancer Res.* **2020**, *80*, 1773–1783. [CrossRef]
50. Gubarkova, E.V.; Sovetsky, A.A.; Zaitsev, V.Y.; Matveyev, A.L.; Vorontsov, D.A.; Sirotkina, M.A.; Matveev, L.A.; Plekhanov, A.A.; Pavlova, N.P.; Kuznetsov, S.S.; et al. OCT-Elastography-Based Optical Biopsy for Breast Cancer Delineation and Express Assessment of Morphological/Molecular Subtypes. *Biomed. Opt. Express* **2019**, *10*, 2244. [CrossRef]
51. Allen, W.M.; Foo, K.Y.; Zilkens, R.; Kennedy, K.M.; Fang, Q.; Chin, L.; Dessauvagie, B.F.; Latham, B.; Saunders, C.M.; Kennedy, B.F. Clinical Feasibility of Optical Coherence Micro-Elastography for Imaging Tumor Margins in Breast-Conserving Surgery. *Biomed. Opt. Express* **2018**, *9*, 6331. [CrossRef]
52. Sirotkina, M.A.; Gubarkova, E.V.; Plekhanov, A.A.; Sovetsky, A.A.; Elagin, V.V.; Matveyev, A.L.; Matveev, L.A.; Kuznetsov, S.S.; Zagaynova, E.V.; Gladkova, N.D.; et al. In Vivo Assessment of Functional and Morphological Alterations in Tumors under Treatment Using OCT-Angiography Combined with OCT-Elastography. *Biomed. Opt. Express* **2020**, *11*, 1365. [CrossRef]
53. Plekhanov, A.A.; Sirotkina, M.A.; Sovetsky, A.A.; Gubarkova, E.V.; Kuznetsov, S.S.; Matveyev, A.L.; Matveev, L.A.; Zagaynova, E.V.; Gladkova, N.D.; Zaitsev, V.Y. Histological Validation of in Vivo Assessment of Cancer Tissue Inhomogeneity and Automated Morphological Segmentation Enabled by Optical Coherence Elastography. *Sci. Rep.* **2020**, *10*, 11781. [CrossRef]
54. Nandy, S.; Salehi, H.S.; Wang, T.; Wang, X.; Sanders, M.; Kueck, A.; Brewer, M.; Zhu, Q. Correlating Optical Coherence Elastography Based Strain Measurements with Collagen Content of the Human Ovarian Tissue. *Biomed. Opt. Express* **2015**, *6*, 3806. [CrossRef]
55. Persu, C.; Chapple, C.R.; Cauni, V.; Gutue, S.; Geavlete, P. Pelvic Organ Prolapse Quantification System (POP-Q)—A new era in pelvic prolapse staging. *J. Med. Life* **2011**, *4*, 4,75–81.
56. Moiseev, A.; Ksenofontov, S.; Sirotkina, M.; Kiseleva, E.; Gorozhantseva, M.; Shakhova, N.; Matveev, L.; Zaitsev, V.; Matveyev, A.; Zagaynova, E.; et al. Optical Coherence Tomography-Based Angiography Device with Real-Time Angiography B-Scans Visualization and Hand-Held Probe for Everyday Clinical Use. *J. Biophotonics* **2018**, *11*, e201700292. [CrossRef]
57. Gelikonov, V.M.; Romashov, V.N.; Shabanov, D.V.; Ksenofontov, S.Y.; Terpelov, D.A.; Shilyagin, P.A.; Gelikonov, G.V.; Vitkin, I.A. Cross-Polarization Optical Coherence Tomography with Active Maintenance of the Circular Polarization of a Sounding Wave in a Common Path System. *Radiophys Quantum El* **2018**, *60*, 897–911. [CrossRef]
58. Sovetsky, A.A.; Matveyev, A.L.; Matveev, L.A.; Gubarkova, E.V.; Plekhanov, A.A.; Sirotkina, M.A.; Gladkova, N.D.; Zaitsev, V.Y. Full-Optical Method of Local Stress Standardization to Exclude Nonlinearity-Related Ambiguity of Elasticity Estimation in Compressional Optical Coherence Elastography. *Laser Phys. Lett.* **2020**, *17*, 065601. [CrossRef]
59. Zaitsev, V.Y.; Matveyev, A.L.; Matveev, L.A.; Gelikonov, G.V.; Sovetsky, A.A.; Vitkin, A. Optimized Phase Gradient Measurements and Phase-Amplitude Interplay in Optical Coherence Elastography. *J. Biomed. Opt.* **2016**, *21*, 116005. [CrossRef]
60. Zaitsev, V.Y.; Matveyev, A.L.; Matveev, L.A.; Gelikonov, G.V.; Gubarkova, E.V.; Gladkova, N.D.; Vitkin, A. Hybrid Method of Strain Estimation in Optical Coherence Elastography Using Combined Sub-Wavelength Phase Measurements and Supra-Pixel Displacement Tracking. *J. Biophoton* **2016**, *9*, 499–509. [CrossRef]
61. Matveyev, A.L.; Matveev, L.A.; Sovetsky, A.A.; Gelikonov, G.V.; Moiseev, A.A.; Zaitsev, V.Y. Vector Method for Strain Estimation in Phase-Sensitive Optical Coherence Elastography. *Laser Phys. Lett.* **2018**, *15*, 065603. [CrossRef]
62. Sovetsky, A.A.; Matveyev, A.L.; Matveev, L.A.; Shabanov, D.V.; Zaitsev, V.Y. Manually-Operated Compressional Optical Coherence Elastography with Effective Aperiodic Averaging: Demonstrations for Corneal and Cartilaginous Tissues. *Laser Phys. Lett.* **2018**, *15*, 085602. [CrossRef]
63. Zaitsev, V.Y.; Ksenofontov, S.Y.; Sovetsky, A.A.; Matveyev, A.L.; Matveev, L.A.; Zykov, A.A.; Gelikonov, G.V. Real-Time Strain and Elasticity Imaging in Phase-Sensitive Optical Coherence Elastography Using a Computationally Efficient Realization of the Vector Method. *Photonics* **2021**, *8*, 527. [CrossRef]
64. Zaitsev, V.Y.; Matveyev, A.L.; Matveev, L.A.; Gubarkova, E.V.; Sovetsky, A.A.; Sirotkina, M.A.; Gelikonov, G.V.; Zagaynova, E.V.; Gladkova, N.D.; Vitkin, A. Practical Obstacles and Their Mitigation Strategies in Compressional Optical Coherence Elastography of Biological Tissues. *J. Innov. Opt. Health Sci.* **2017**, *10*, 1742006. [CrossRef]
65. Gubarkova, E.V.; Sovetsky, A.A.; Zaitsev, V.Y.; Matveev, L.A.; Matveyev, A.L.; Vorontsov, D.A.; Timofeeva, L.B.; Kiseleva, E.B.; Vorontsov, A.Y.; Kuznetsova, I.A.; et al. Comparison of Elastic Properties of Tissue Samples in Various Pathological States Using Optical Coherence Elastography. In *Proceedings of the Saratov Fall Meeting 2018: Optical and Nano-Technologies for Biology and Medicine*; Tuchin, V.V., Genina, E.A., Eds.; SPIE: Saratov, Russian Federation; p. 14.
66. Sovetsky, A.A.; Matveyev, A.L.; Matveev, L.A.; Gelikonov, G.V.; Zaitsev, V.Y. Mapping Large Strains in Phase-Sensitive OCT: Key Role of Supra-Pixel Displacement Tracking in Incremental Strain Evaluation. *J. Biomed. Photonics Eng.* **2022**, *8*, 1–16. [CrossRef]
67. Schindelin, J.; Arganda-Carreras, I.; Frise, E.; Kaynig, V.; Longair, M.; Pietzsch, T.; Preibisch, S.; Rueden, C.; Saalfeld, S.; Schmid, B.; et al. Fiji: An Open-Source Platform for Biological-Image Analysis. *Nat. Methods* **2012**, *9*, 676–682. [CrossRef]
68. Ruifrok, A.C.; Katz, R.L.; Johnston, D.A. Comparison of Quantification of Histochemical Staining By Hue-Saturation-Intensity (HSI) Transformation and Color-Deconvolution. *Appl. Immunohistochem. Mol. Morphol.* **2003**, *11*, 85–91. [CrossRef]
69. Otsu, N. A Threshold Selection Method from Gray-Level Histograms. *IEEE Trans. Syst. Man Cybern.* **1979**, *9*, 62–66. [CrossRef]

70. Saito, T.; Toriwaki, J.-I. New Algorithms for Euclidean Distance Transformation of an N-Dimensional Digitized Picture with Applications. *Pattern Recognit.* **1994**, *27*, 1551–1565. [CrossRef]
71. Hildebrand, T.; Rüegsegger, P. A New Method for the Model-independent Assessment of Thickness in Three-dimensional Images. *J. Microsc.* **1997**, *185*, 67–75. [CrossRef]
72. Ushiki, T. Collagen Fibers, Reticular Fibers and Elastic Fibers. A Comprehensive Understanding from a Morphological Viewpoint. *Arch. Histol. Cytol.* **2002**, *65*, 109–126. [CrossRef]
73. Egorov, V.; van Raalte, H.; Lucente, V. Quantifying Vaginal Tissue Elasticity under Normal and Prolapse Conditions by Tactile Imaging. *Int. Urogynecol. J.* **2012**, *23*, 459–466. [CrossRef]
74. Li, C.; Guan, G.; Ling, Y.; Hsu, Y.-T.; Song, S.; Huang, J.T.-J.; Lang, S.; Wang, R.K.; Huang, Z.; Nabi, G. Detection and Characterisation of Biopsy Tissue Using Quantitative Optical Coherence Elastography (OCE) in Men with Suspected Prostate Cancer. *Cancer Lett.* **2015**, *357*, 121–128. [CrossRef]
75. Deng, Z.-M.; Dai, F.-F.; Yuan, M.-Q.; Yang, D.-Y.; Zheng, Y.-J.; Cheng, Y.-X. Advances in Molecular Mechanisms of Pelvic Organ Prolapse (Review). *Exp. Ther. Med.* **2021**, *22*, 1009. [CrossRef]
76. De Landsheere, L.; Munaut, C.; Nusgens, B.; Maillard, C.; Rubod, C.; Nisolle, M.; Cosson, M.; Foidart, J.-M. Histology of the Vaginal Wall in Women with Pelvic Organ Prolapse: A Literature Review. *Int. Urogynecol. J.* **2013**, *24*, 2011–2020. [CrossRef]
77. Borges, L.F.; Gutierrez, P.S.; Marana, H.R.C.; Taboga, S.R. Picrosirius-Polarization Staining Method as an Efficient Histopathological Tool for Collagenolysis Detection in Vesical Prolapse Lesions. *Micron* **2007**, *38*, 580–583. [CrossRef]
78. Lin, S.-Y.; Tee, Y.-T.; Ng, S.-C.; Chang, H.; Lin, P.; Chen, G.-D. Changes in the Extracellular Matrix in the Anterior Vagina of Women with or without Prolapse. *Int. Urogynecol. J.* **2007**, *18*, 43–48. [CrossRef]
79. Kökçü, A.; Yanik, F.; Çetinkaya, M.; Alper, T.; Kandemir, B.; Malatyalioglu, E. Histopathological Evaluation of the Connective Tissue of the Vaginal Fascia and the Uterine Ligaments in Women with and without Pelvic Relaxation. *Arch. Gynecol. Obstet.* **2002**, *266*, 75–78. [CrossRef]
80. Moalli, P.A.; Shand, S.H.; Zyczynski, H.M.; Gordy, S.C.; Meyn, L.A. Remodeling of Vaginal Connective Tissue in Patients With Prolapse. *Obstet. Gynecol.* **2005**, *106*, 953–963. [CrossRef]
81. Ouchi, M.; Kato, K.; Gotoh, M.; Suzuki, S. Physical activity and pelvic floor muscle training in patients with pelvic organ prolapse: A pilot study. *Int. Urogynecol. J.* **2017**, *28*, 1807–1815. [CrossRef]
82. Porta-Roda, O.; Vara-Paniagua, J.; Díaz-López, M.A.; Sobrado-Lozano, P.; Simó-González, M.; Díaz-Bellido, P.; Reula-Blasco, M.C.; Muñoz-Garrido, F. Effect of Vaginal Spheres and Pelvic Floor Muscle Training in Women with Urinary Incontinence: A Randomized, Controlled Trial: Vaginal Spheres in Urinary Incontinence. *Neurourol. Urodynam.* **2015**, *34*, 533–538. [CrossRef] [PubMed]
83. Deng, M.; Ding, J.; Ai, F.; Zhu, L. Successful Use of the Gellhorn Pessary as a Second-Line Pessary in Women with Advanced Pelvic Organ Prolapse. *Menopause* **2017**, *24*, 1277–1281. [CrossRef] [PubMed]
84. Friedman, T.; Eslick, G.D.; Dietz, H.P. Risk Factors for Prolapse Recurrence: Systematic Review and Meta-Analysis. *Int. Urogynecol. J.* **2018**, *29*, 13–21. [CrossRef] [PubMed]
85. Zhang, L.; Yaron, J.R.; Tafoya, A.M.; Wallace, S.E.; Kilbourne, J.; Haydel, S.; Rege, K.; McFadden, G.; Lucas, A.R. A Virus-Derived Immune Modulating Serpin Accelerates Wound Closure with Improved Collagen Remodeling. *JCM* **2019**, *8*, 1626. [CrossRef]
86. Belsare, A.D.; Mushrif, M.M.; Pangarkar, M.A.; Meshram, N. Classification of Breast Cancer Histopathology Images Using Texture Feature Analysis. In Proceedings of the TENCON 2015—2015 IEEE Region 10 Conference, Macao, 1–4 November 2015; IEEE: Piscataway, NJ, USA; pp. 1–5.
87. Liu, Y.; Dong, Y.; Si, L.; Meng, R.; Dong, Y.; Ma, H. Comparison between Image Texture and Polarization Features in Histopathology. *Biomed. Opt. Express* **2021**, *12*, 1593. [CrossRef]
88. Möckl, L.; Lamb, D.C.; Bräuchle, C. Super-Resolved Fluorescence Microscopy: Nobel Prize in Chemistry 2014 for Eric Betzig, Stefan Hell, and William E. Moerner. *Angew. Chem. Int. Ed.* **2014**, *53*, 13972–13977. [CrossRef]
89. de Landsheere, L.; Brieu, M.; Blacher, S.; Munaut, C.; Nusgens, B.; Rubod, C.; Noel, A.; Foidart, J.-M.; Nisolle, M.; Cosson, M. Elastin Density: Link between Histological and Biomechanical Properties of Vaginal Tissue in Women with Pelvic Organ Prolapse? *Int. Urogynecol. J.* **2016**, *27*, 629–635. [CrossRef]